Title
How much global burned area can be forecast on seasonal time scales using sea surface temperatures?

Journal
Environmental Research Letters, 11(4)

ISSN
1748-9318

Authors
Chen, Yang
Morton, Douglas C
Andela, Niels
et al.

Publication Date
2016-04-01

DOI
10.1088/1748-9326/11/4/045001

Peer reviewed

How much global burned area can be forecast on seasonal time scales using sea surface temperatures?

2016 Environ. Res. Lett. 11 045001

(http://iopscience.iop.org/1748-9326/11/4/045001)

Environmental Research Letters

PAPER

How much global burned area can be forecast on seasonal time scales using sea surface temperatures?

Yang Chen[1], Douglas C Morton[2], Niels Andela[2], Louis Giglio[3] and James T Randerson[1]

[1] Department of Earth System Science, University of California, Irvine, CA 92697, USA
[2] Biospheric Sciences Branch, NASA Goddard Space Flight Center, Greenbelt, MD 20771, USA
[3] Department of Geographical Sciences, University of Maryland, College Park, MD 20742, USA

E-mail: yang.chen@uci.edu

Keywords: biomass burning, teleconnection, seasonal outlook, mitigation

Supplementary material for this article is available online

OPEN ACCESS

RECEIVED
23 November 2015

REVISED
23 February 2016

ACCEPTED FOR PUBLICATION
3 March 2016

PUBLISHED
23 March 2016

Abstract

Large-scale sea surface temperature (SST) patterns influence the interannual variability of burned area in many regions by means of climate controls on fuel continuity, amount, and moisture content. Some of the variability in burned area is predictable on seasonal timescales because fuel characteristics respond to the cumulative effects of climate prior to the onset of the fire season. Here we systematically evaluated the degree to which annual burned area from the Global Fire Emissions Database version 4 with small fires (GFED4s) can be predicted using SSTs from 14 different ocean regions. We found that about 48% of global burned area can be forecast with a correlation coefficient that is significant at a $p < 0.01$ level using a single ocean climate index (OCI) 3 or more months prior to the month of peak burning. Continental regions where burned area had a higher degree of predictability included equatorial Asia, where 92% of the burned area exceeded the correlation threshold, and Central America, where 86% of the burned area exceeded this threshold. Pacific Ocean indices describing the El Niño-Southern Oscillation were more important than indices from other ocean basins, accounting for about 1/3 of the total predictable global burned area. A model that combined two indices from different oceans considerably improved model performance, suggesting that fires in many regions respond to forcing from more than one ocean basin. Using OCI—burned area relationships and a clustering algorithm, we identified 12 hotspot regions in which fires had a consistent response to SST patterns. Annual burned area in these regions can be predicted with moderate confidence levels, suggesting operational forecasts may be possible with the aim of improving ecosystem management.

1. Introduction

Seasonal forecasting of landscape fire activity is a relatively new endeavor that has become possible with recent improvements in the quality of fire and climate time series. Physically-based forecast models (e.g. Roads *et al* 2005, 2010, Spessa *et al* 2015) predict the evolution of local climate variables before and during the fire season. Together with various human influences such as land-use change and fire suppression, these climate variables are used to create a measurable prediction of fire risk (Field *et al* 2015). Another type of forecast model relies on statistical correlations between fire and local or large-scale climate patterns prior to the onset of the fire season (e.g. Westerling *et al* 2002, Preisler and Westerling 2007, Riano *et al* 2007, Field and Shen 2008, Dixon *et al* 2008, Chen *et al* 2011, Preisler *et al* 2011, Shabbar *et al* 2011, Gudmundsson *et al* 2014, Marcos *et al* 2015). Major climate variables used in these models include precipitation, temperature, soil moisture, sea surface temperature (SST), and composite indicators such as the Palmer Drought Severity Index (Alley 1984). Regional climate indices may yield some predictive skill even in locations where local climate–fire associations are not strong (Westerling *et al* 2002).

Recent studies have shown that large-scale ocean-climate teleconnection patterns can influence fire occurrence in many regions, highlighting the potential of SSTs from three major oceans (Pacific, Atlantic, and

Indian) to provide an '*a priori*' estimate of fire season severity. El Niño Southern-Oscillation (ENSO) and Pacific Decadal Oscillation (PDO), for example, are known to significantly influence wildfires in North America (Duffy *et al* 2005, Schoennagel *et al* 2005, Liu 2006, Macias Fauria and Johnson 2006, Kitzberger *et al* 2007, Macias Fauria and Johnson 2008, Goodrick and Hanley 2009, Shabbar *et al* 2011). Strong El Niño conditions also alter precipitation and other fire weather variables that control the magnitude of fire activity in equatorial Asia (Field *et al* 2009, van der Kaars *et al* 2010, Barbero *et al* 2011, Reid *et al* 2012, Wooster *et al* 2012), Southeast Asia (Fuller and Murphy 2006), the eastern Amazon basin (Alencar *et al* 2011), and Africa (Andela and van der Werf 2014). In regions such as the Amazon (Chen *et al* 2011, Fernandes *et al* 2011), southeastern US (Dixon *et al* 2008), Canada (Skinner *et al* 2006), and Indonesia (Field and Shen 2008), fires may be affected by teleconnections initiated from multiple oceans.

Processes that link SSTs and fire behavior are complex. Fires may respond to SST variations at or before the onset of the fire season, and the climate influence can occur by means of multiple pathways. Fuel continuity, amount, and the moisture content of live and dead fuel are sensitive to climate regulation of net primary production (NPP) and soil moisture prior to the fire season (Hessl 2011). NPP and soil moisture, in turn, respond to the integrated effects of precipitation anomalies and climate variables that regulate evapotranspiration, species composition, and mortality. Climate prior to the fire season also likely influences land manager expectations and burning decisions in many areas, although these types of interactions are not well understood. In temperate and boreal ecosystems, snow cover and depth may serve as a capacitor influencing ecosystem moisture levels during the following fire season (Westerling *et al* 2006). In other areas, SSTs may influence ecosystem moisture levels over such a large area that land-atmosphere feedbacks are modified in subsequent seasons. For example, in the Amazon, Chen *et al* (2013) found that lower cumulative precipitation (which is linked to anomalously high SSTs in the tropical North Atlantic and tropical eastern Pacific) reduces terrestrial water storage in forest ecosystems by the end of the wet season. Reduced soil moisture reserves subsequently limit evapotranspiration during the following dry season, causing atmospheric humidity to drop within the basin, and thus enabling forest fires to spread more easily through the understory (Morton *et al* 2013).

Although many studies have explored the relationship between SSTs and fire activity for specific land regions, a global perspective on SST–fire relationships has remained elusive due to the lack of consistent global fire time series. With over 18 years of burned area observations (1997–2015) (Giglio *et al* 2013) from the Global Fire Emissions Database (GFED) (van der Werf *et al* 2010), a systematic analysis of SST–fire relationships across different continents and biomes is now possible. For the first time, we evaluated the degree to which seasonal burned area forecasts can be developed in different regions using SSTs as statistical predictors. We used 14 ocean climate indices (OCIs) that represent the mean or spatial gradient of SSTs in different ocean regions. These OCIs were produced on a weekly or monthly basis by different centers at the National Oceanic and Atmospheric Administration (NOAA)—making them a suitable for operational forecasts. In a first step, we explored the strength of the coupling between individual OCIs and satellite-observed burned area, and identify fire regions that are significantly affected by each of these OCIs. We then constructed statistical forecast models for burned area in each grid cell using the optimal correlations between OCIs and GFED burned area time series. Using a clustering algorithm, we identified 'hotspot' regions where the sensitivities of burned area to different OCIs were consistent and the seasonal predictability was high. Our results highlight the significant global influence of OCIs on interannual variability in burned area, and identify specific regions where it may be possible to develop operational fire forecasts using OCI information. Uncertainties related to the data and approach, as well as potential directions for future research, are presented in the discussion.

2. Data and methods

2.1. Burned area

To quantify interannual variability in global fires, we used the fourth version of GFED burned area product (Giglio *et al* 2013) updated to account for small fires (GFED4s, Randerson *et al* 2012). We extended GFED4s burned area estimates to the pre-MODIS era using the relationship between GFED4s and Visible and Infrared Scanner and European Space Agency Advanced Along Track Scanning Radiometer active fire detections. We used monthly GFED4s data to calculate annual burned area at 1° resolution (figure 1) in each fire year, a 12-month period centered on the peak fire month (figure S1(A)). Drawing on monthly observations from July 1996 through May 2015, the total length of the full annual burned area time series we analyzed was 18 years, from 1997 through 2014. Important uncertainties in the burned area time series originate from challenges in detecting and representing the statistics of burned area from fires that are smaller from the 500 m resolution of the MODIS surface reflectance product (Randerson *et al* 2012) and from fusing fire records from the MODIS era (2001–2015) with thermal anomaly time series from the pre-MODIS era (1996–2000) (Giglio *et al* 2013).

2.2. Ocean climate indices

We examined 14 OCIs representing SST status in three oceans: the Pacific, the Atlantic, and the Indian Ocean

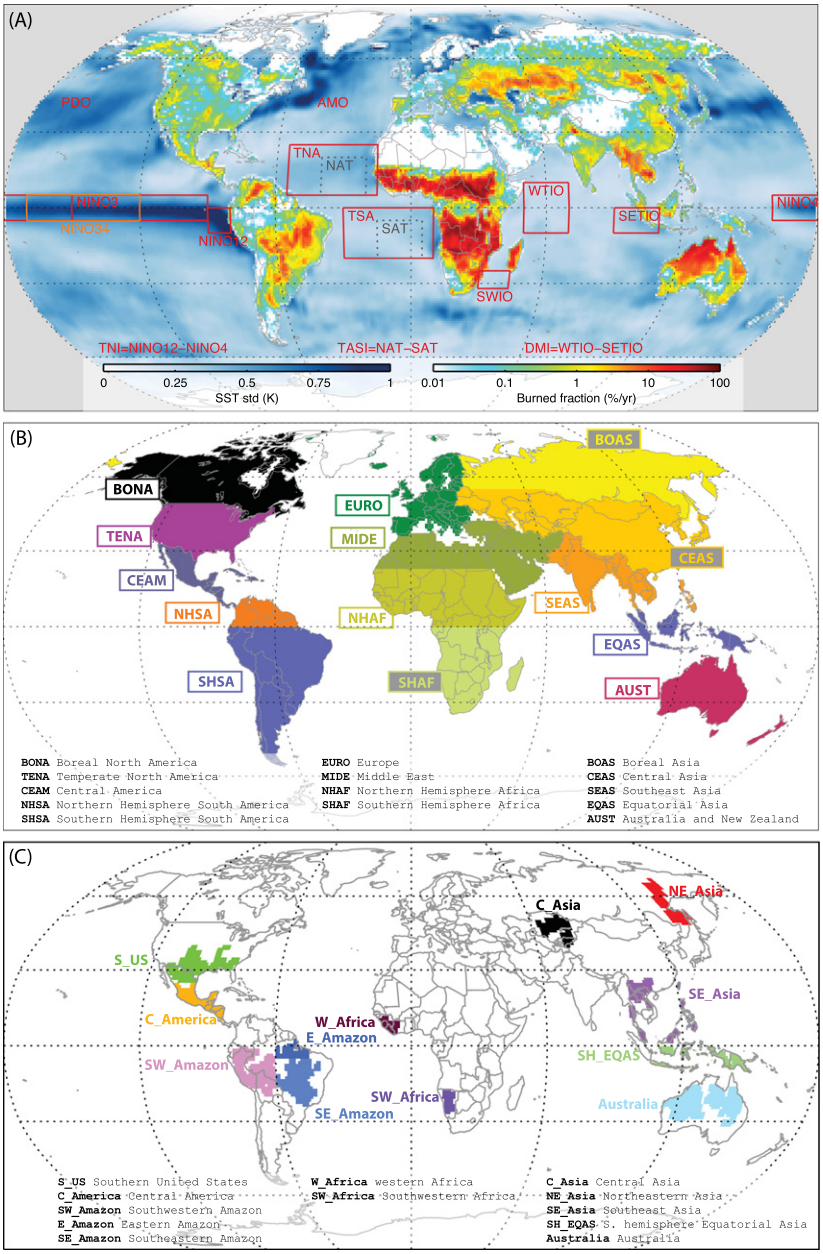

Figure 1. (A) Location of the 14 ocean climate index (OCI) regions used in this study. The full names and area coverage of the different OCIs are described in table S1. The mean annual burned fraction (%/yr) over 1997–2014 is shown on land, and the SST interannual variability (standard deviation, in K) during 1995–2014 is shown on the ocean, which was derived after removing a climatological annual mean cycle. (B) Regions used for aggregated statistics reported in tables 1 and S2. Boundaries of the regions were derived from the Global Fire Emissions Database (GFED), after Giglio *et al* (2006), van der Werf *et al* (2006), and van der Werf *et al* (2010). (C) Location of the 12 hotspot regions where burned area had a relatively high degree of predictability and had a coherent response to the same OCIs.

(figures 1(A), S2, and table S1). Eleven 'magnitude' OCIs are mean SST anomalies over specific regions representing SST variability in the Pacific (PDO, NINO4, NINO34, NINO3, and NINO12), Atlantic (TNA, TSA, and AMO), and Indian Oceans (SWIO, WTIO, and SETIO). Three 'gradient' OCIs (TNI, TASI, and DMI) were calculated as the difference of OCIs for two regions within the same ocean basin. We downloaded monthly time series of the OCIs in NetCDF format from NOAA's State of the Ocean website (http://stateoftheocean.osmc.noaa.gov/). Evidence for a range of covariance relationships among OCIs (figure S3) was used to restrict 2-OCI models to indices from different ocean basins.

2.3. Cross correlation analyses and optimal regression models

For each 1° × 1° grid cell where annual BA was non-zero in at least 9 of the 18 years during our study period, we examined the linear correlation between burned area and each OCI, with the OCI leading the peak fire month by a period of between 3 and 12 months. A minimum lead time of 3 months (ahead of the peak fire month) was selected recognizing that

forecasts are likely to be more useful to land managers when there is adequate time to plan and adjust resources prior to the onset of the fire season. The largest positive or negative correlation values (and the associated lead times) were recorded for each OCI. Among different OCIs, we selected the regression model with the highest absolute values of correlation as our optimal 1-OCI model ($BA = aOCI_1 + c$). In order to examine the ENSO contribution to fire predictability, we derived a similar 1-OCI optimal model that used only the four NINO indices.

We also created a 2-OCI model ($BA = aOCI_1 + bOCI_2 + c$) for each grid cell by combining information from two OCIs representing different ocean basins. The a, b, and c coefficients were obtained from least squares linear regression. In constructing the 2-OCI model, we forced the first OCI and its lead time to be the same as the optimal 1-OCI model, and then selected an additional OCI from another ocean basin that, combined with the first OCI, explained the largest amount of variability in the observed burned area time series.

We calculated Pearson's correlation coefficient (r) between gridded burned area from historical observations and the burned area predicted using the optimal models. The burned area in a grid cell was assumed to be predictable if $r > 0.59$ (corresponding to $p < 0.01$, $n = 18$). For each of the 14 land regions used in GFED (figure 1(B)), we quantified the average predictability for the region as a whole by calculating the fraction of regional burned area that occurred in grid cells where burned area was predictable at a level of $p < 0.01$ (fBA). As another indicator of predictability, we calculated the mean r^2 value (weighted by burned area in each grid cell) of the 1-OCI and 2-OCI models for each GFED region.

2.4. Clustering analysis and model evaluation in hotspot regions

We used the k-means algorithm (Pena *et al* 1999) to identify clusters of grid cells that exhibited a high degree of predictability ($p < 0.01$) and responded in similar ways to the global set of OCIs. Inputs to the clustering method included the optimal correlation coefficients and the optimal lead times (in months) from linear regression between burned area and each of the single OCIs. The total number of clusters was set to be 15, although sensitivity tests generated a similar spatial pattern of clusters if we chose a different parameter value. By performing ensemble runs of the clustering algorithm (Text S1), we derived 12 hotspot regions globally (figure 1(C)), which represented spatially contiguous regions where it may be possible to develop operational fire forecasts with moderate levels of predictability.

For each of these hotspots, we created a single merged burned area time series and then derived optimal 1-OCI and 2-OCI models, similar to the approach described above for our gridded analysis. The skill of the forecast model was evaluated using a cross-validation approach in which the data were divided into 'learning' and 'validation' data sets (von Storch and Zwiers 2001). In the cross-validation, we constructed a 'leave-one-out' model in which the model parameters used to calculate the burned area in a target year were derived from data in all other years. Given that fires in some regions have a nonlinear response to precipitation anomalies (van der Werf *et al* 2008), we also tested whether a nonlinear model could improve the level of fire predictability in these hotspots regions. The nonlinear model was similar to the optimal 2-OCI model except with optimized parameters to fit the natural logarithm of burned area: $\ln(BA) = aOCI_1 + bOCI_2 + c$.

3. Results

3.1. Influence of individual OCIs on global burned area variability

Pacific OCIs, representing the ENSO and PDO modes of climate variability, influenced landscape fires across multiple continents (table 1). Important regions of positive influence included tropical and boreal Asia, Central and South America, and East Africa (figure 2). Regions where the Pacific OCIs had a negative influence included Australia, India, southern Africa, and southern South America.

In boreal, temperate, and equatorial Asia, eastern Pacific OCIs (e.g., NINO12) had a stronger positive influence on burned area than western Pacific OCIs (e.g., NINO4), implying that eastern Pacific El Niño events (Kao and Yu 2009) may have a stronger regional teleconnection with climate variables that influence burned area. For fire prone savanna regions in western and northern Australia, stronger negative correlations with long lead times were found for western Pacific OCIs. This pattern is consistent with ENSO-driven reductions in precipitation and fuel build-up during the growing season, thereby limiting rates of fire spread in the following dry season.

Fires in Central and South America also were sensitive to Pacific SSTs. In most of southern hemispheric tropical South America, Pacific OCIs with 3–10 month lead times were positively correlated with burned area, similar to previous reports of a positive relationship between Ocean Niño Index and satellite-derived active fire detections in the southern Amazon (Chen *et al* 2011). Western Pacific OCIs had a stronger positive influence on burned area in South America, whereas central and eastern Pacific OCIs were more important predictors for Central America.

In general, fires in extratropical regions were less sensitive to Pacific OCIs than those in tropical forests and savannas, with several notable exceptions. NINO4 had positive correlation with burned area in grasslands in Central Asia. In the agricultural belt across southern

Table 1. The percentage of burned area in each GFED region that can be predicted using OCI-based statistical models with a lead time ⩾3 months. At each 1° × 1° grid cell within a region, burned area was denoted as 'predictable' if the OCI—burned area correlation was significant at a $p < 0.01$ level ($r > 0.59$). For each region, the highest OCI—burned area relationship is highlighted in bold. The 1-OCI, 1-OCI NINOs and 2-OCI models used different OCI information in each 1° × 1° grid cell. The NINOs fraction represents the ratio of the predictable burned area from the 1-OCI NINOs only model to that from the full 1-OCI model. This metric provides a measure of the importance of ENSO in regulating burned area variability.

	Fixed-OCI model																
	Pacific						**Atlantic**				**Indian**				Combined models		
Region	NINO4	NINO34	NINO3	NINO12	PDO	TNI	TNA	TSA	AMO	TASI	SWIO	WTIO	SETIO	DMI	1-OCI	2-OCI	NINOs fraction
BONA	14	17	20	22	21	21	20	21	17	18	**23**	20	20	22	47	83	0.49
TENA	4	1	1	4	3	2	**20**	3	9	3	9	2	5	10	52	96	0.17
CEAM	3	28	47	**58**	32	44	6	58	1	9	14	29	52	53	86	99	0.71
NHSA	7	12	9	10	**15**	4	14	6	9	9	3	1	5	5	43	96	0.40
SHSA	9	15	11	8	14	1	14	4	19	8	5	**24**	8	9	58	97	0.34
EURO	2	0	1	1	7	1	5	1	3	5	8	2	**9**	4	29	97	0.10
MIDE	9	11	10	8	**19**	8	9	7	10	7	7	15	10	9	50	98	0.38
NHAF	2	2	6	15	6	**18**	4	4	6	6	5	7	6	8	51	97	0.35
SHAF	3	4	7	9	7	**13**	4	7	4	6	2	11	7	5	45	96	0.31
BOAS	3	3	9	12	**16**	10	9	8	3	5	11	6	12	12	41	92	0.34
CEAS	3	1	3	3	**7**	4	5	3	3	7	7	4	4	6	33	93	0.18
SEAS	7	9	10	**14**	8	11	7	4	4	5	6	5	3	14	54	97	0.35
EQAS	14	65	**65**	20	68	7	0	52	1	54	61	56	9	6	92	99	0.79
AUST	7	4	1	1	8	1	**12**	5	4	4	4	4	9	3	41	98	0.22
GLOBE	4	5	7	11	8	**13**	6	6	6	6	4	9	7	7	48	97	0.33

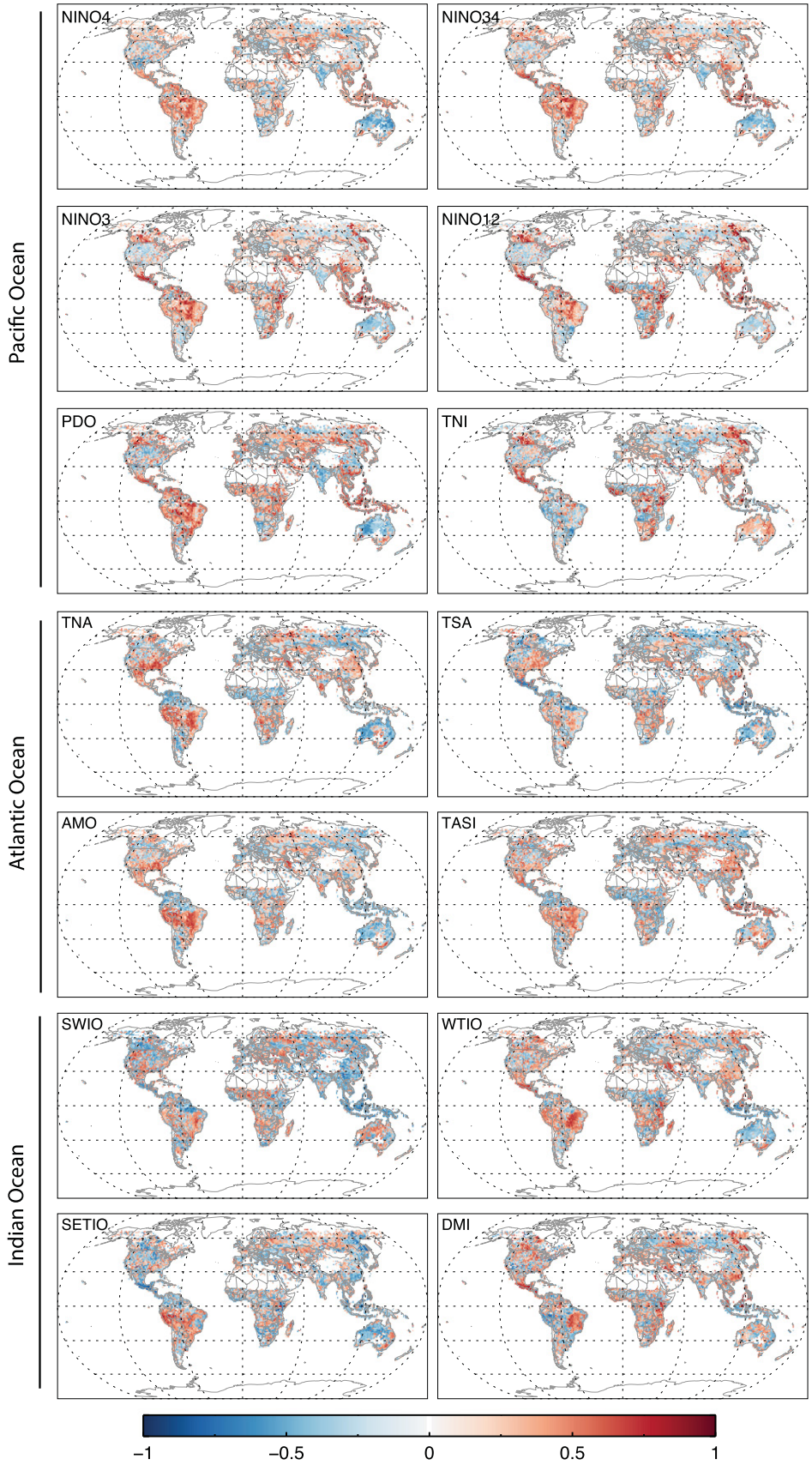

Figure 2. Maximum correlation between burned area and each OCI, grouped according to ocean basin. The correlation coefficient with the largest absolute value is shown, with lead times varying between 3 and 12 months. Red and blue colors indicate positive and negative correlations, respectively. Figure S4 provides a map of the corresponding lead times.

Canada, OCIs in the central and eastern Pacific (NINO3 and NINO12) were positively correlated with burned area.

Atlantic OCIs were important in explaining burned area across North and South America and in several more remote areas. A positive relationship was found between North Atlantic OCIs (AMO and TNA) and fires in tropical South America (figure 2). TNA was also a strong positive driver of burned area in the southeastern US, whereas TSA had a moderate negative impact on burned area in Central America. Tropical Atlantic OCIs (TNA and TSA) also had a moderate role in influencing burned area in several remote regions within northern Asia, Southeast Asia, and Australia.

All three magnitude OCIs in the Indian Ocean had a negative influence on burned area in Indonesia (figure 2), but with different lead times (figure S4). The two components of the Indian Ocean dipole, WTIO and SETIO, had opposing impacts on burned areas in East Africa. Positive phases of WTIO increased burned area, whereas positive phases of SETIO had the opposite effect. Likely because some OCIs in the Indian Ocean co-varied (and lagged behind) Pacific OCIs, they also had high levels of correlation with burned areas in several other remote regions, including South America.

3.2. Using statistical models to predict regional and global burned area

Globally, about 48% of burned area was predictable with a lead time of 3 or more months (with $r > 0.59$ and $p < 0.01$) (table 1 and figure S5(C)). Equatorial Asia had the largest fractions of predictable burned area using an optimized 1-OCI model (92%), followed by Central America (86%). In contrast, Europe and Central Asia had the lowest fractions of predictable burned area at 29% and 33%, respectively. The fraction of predictable burned area in other regions varied between 41% and 58%. The 1-OCI model separately selected the optimal OCI in each 1° grid cell, capturing heterogeneous regional patterns in OCI–fire relationships (figure S5), thereby predicting a greater fraction of burned area in each GFED region than a regionally invariant OCI model (table 1).

At a global scale, about a third of predictable burned area can be directly linked with ENSO dynamics (figure S6 and table 1). Equatorial Asia and Central America were the two regions with the highest ENSO influence, whereas temperate North America and Europe had relatively low levels of influence, based on the ratio of models using only the four NINO OCIs to optimized 1-OCI model using all 14 OCIs (table 1). Considering a burned area-weighted global mean r^2 value as a separate metric of predictability, we found that the NINO-only model accounted for 63% of the predictable variance obtained from a baseline model constructed from all of the OCIs (table S2).

Using a 2-OCI model, the correlation between observed burned area and predicted burned increased substantially in many grid cells (figure S5), and the fraction of predictable burned area increased at a global scale to 97% (table 1). This suggests that fires in many regions respond to forcing from more than one ocean basin. While this has been demonstrated in prior work for specific regions (e.g. Skinner *et al* 2006, Dixon *et al* 2008, Chen *et al* 2011, Fernandes *et al* 2011), this is the first analysis that shows dual forcing of burned area is prevalent at a global scale.

The fraction of predictable burned area was sensitive to the threshold used to define a significant relationship and the lead time. Figure 3 shows that *f*BA values in most regions were over 80% for a threshold of $r > 0.47$ (corresponding to $p < 0.05$) for the single OCI model, and above 95% for the 2-OCI model. Considering a more stringent criterion of $r > 0.71$ ($p < 0.001$), the fractions of predictable burned area remained high for equatorial Asia and Central America, but were considerably reduced in other regions. Predictable fractions of burned area also were reduced as lead times increased, a key consideration for fire forecasting applications.

3.3. Fire predictability in hotspot regions

We identified 12 hotspot regions where operational fire forecasts may be possible using OCIs (figure 1(C) and table 2). For these regions, a 2-OCI model explained between 57% and 85% of the burned area variance. The 2-OCI model was a substantial improvement over a 1-OCI model in all hotspot regions except southern hemispheric equatorial Asia (SH_EQAS) and northeastern Asia (NE_Asia), likely because a single climate mode (ENSO) has a dominant influence on interannual burned area variability in these regions.

A cross validation analysis confirmed that the 2-OCI model was robust in many hotspot regions, including the Amazon, western Africa, Southeast Asia, and Australia (figure 4). However, where a single peak dominated burned area time series (such as 1997–1998 El Niño impacts on burned area in Central America and northeastern Asia), the cross-validation model was not able to capture these events, resulting in lower correlation metrics (table 2).

Nonlinear (exponential) models considerably improved model performance in about half of the hotspot regions, with the same degrees of freedom (table 2). The largest improvement was observed in southern hemisphere equatorial Asia (r increases from 0.86 to 0.94), consistent with the strong nonlinearity between fire emissions and drought described in van der Werf *et al* (2008). The cross validation exponential model also had better predictive ability in the southern US, northeastern Asia, and southern hemisphere equatorial Asia.

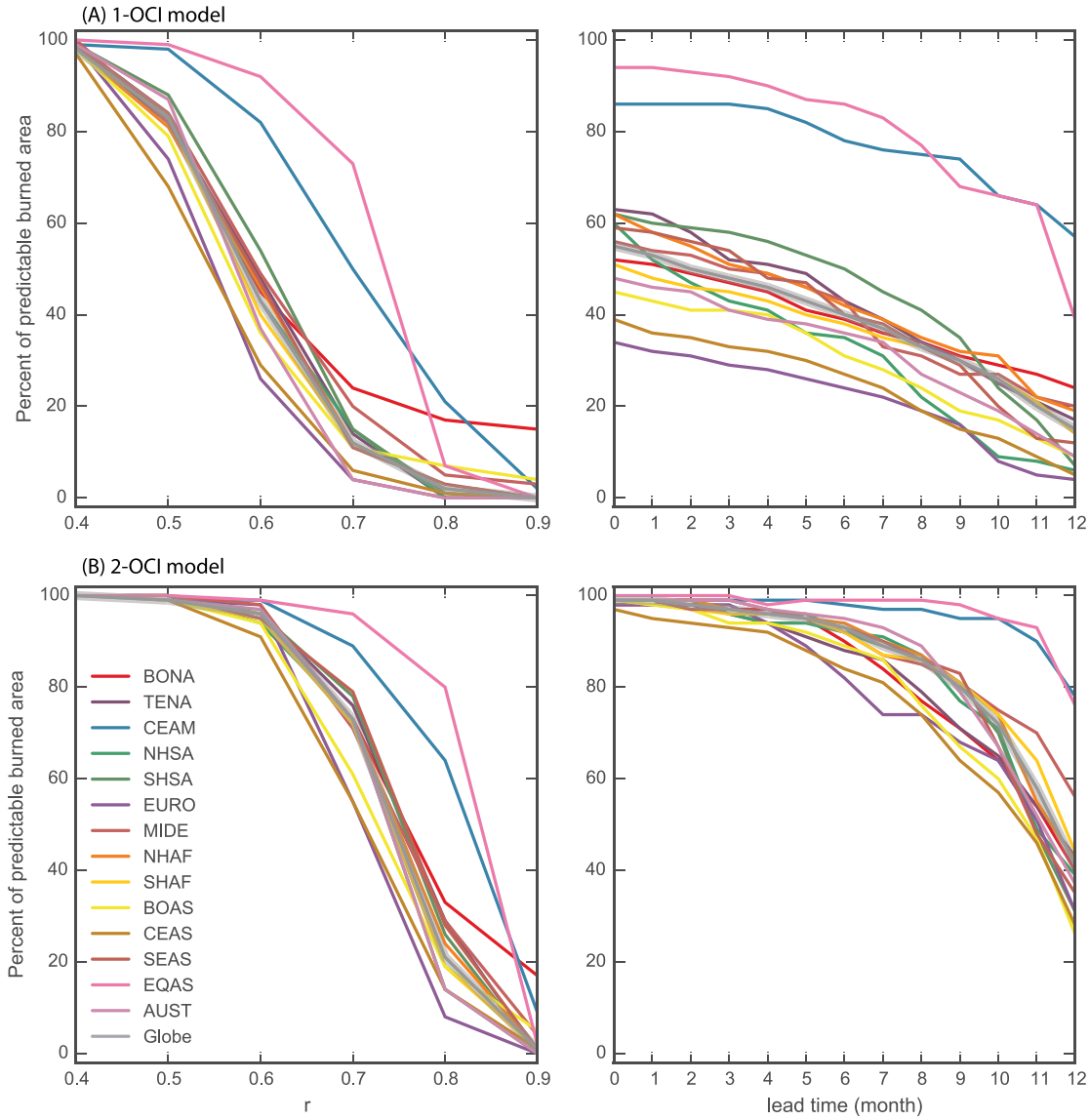

Figure 3. The percentage of predictable burned area in each GFED region as a function of the correlation threshold (left panels, with lead time of 3 months) or as a function of the lead time (right panels, with a correlation threshold of $r > 0.59$, or $p < 0.01$).

4. Discussion

Globally, 48% of burned area can be predicted with 3–12 month lead times using a single OCI. ENSO was the strongest single predictor of interannual variability in global burned area, yet a 2-OCI model doubled the amount of predictable global burned area compared with the 1-OCI approach. The sensitivity of burned area dynamics in most GFED regions to OCI dynamics in two ocean basins suggests that a range of mechanisms link climate modes and fire activity in the Earth system, including teleconnections with different lead times, synchronizing burned area anomalies across large areas. Analysis of burned area variability also revealed specific hotspot regions with strong and consistent responses to specific OCIs. These hotspot regions may be suitable for further development of operational fire forecasts and related investigations of the mechanisms that link OCI and fire activity. Several important burning regions were notably absent from the hotspot analysis, however, including frequently burning areas of sub-Saharan Africa. Regions with substantial burned area but low interannual variability (see figure S1) constitute a challenge for fire forecast systems based solely on OCI data.

4.1. Hotspots of burned area predictability

Several of the hotspots we identified in our global analysis overlap spatially with existing efforts to develop operational fire forecasts. For example, Spessa *et al* (2015) recently developed a seasonal fire and haze forecasting system in southern Kalimantan of Indonesia using model predictions of rainfall. An early warning system is particularly important for the Indonesian peatland fires because of their impacts on the air quality of densely populated neighboring areas (Marlier *et al* 2013, Aouizerats *et al* 2015). Our analysis suggests that it may be possible to develop seasonal fire

Table 2. Model parameters (optimal OCIs and associated lead times, lt) and evaluation metrics (Pearson's correlation, *r*, and the Akaike information criterion, AIC) in different hotspot regions. The models were optimized from linear regressions between total annual burned area in each region and different combinations of OCIs and lead times. The first OCI and its lead time in 2-OCI models were the same as the optimal OCI used in the 1-OCI model. We used AIC (Akaike 1974) to assess tradeoffs between performance and complexity of the 1-OCI and the 2-OCI models. The preferable model is the one with smallest AIC value. For the 2-OCI model, we also report results from a nonlinear (exponential) model. In the cross-validation analysis, the target year was not used in developing the model parameters used to predict burned area in that year.

					2-OCI model							
					Standard						Cross-validation	
	1-OCI linear model				Linear					Nonlinear	Linear	Nonlinear
Hotspot region	OCI	lt	*r*	AIC	OCI(2)	lt(2)	*r*(2)	*r*	AIC	*r*	*r*	*r*
S_US	TNA	10	0.68	34.7	WTIO	10	−0.55	0.86	26.8	0.82	0.39	0.55
C_America	NINO12	4	0.81	62.8	SWIO	9	0.41	0.87	60.1	0.90	0.33	0.30
SW_Amazon	AMO	4	0.76	66.3	SWIO	10	−0.13	0.88	59.8	0.85	0.84	0.79
E_Amazon	PDO	3	0.77	25.1	SWIO	8	−0.47	0.85	20.1	0.90	0.63	0.87
SE_Amazon	WTIO	9	0.69	119.9	TSA	12	0.17	0.79	110.3	0.82	0.64	0.71
W_Africa	TNI	3	0.81	67.7	TASI	6	−0.31	0.87	65.0	0.87	0.75	0.78
SW_Africa	SETIO	8	−0.65	65.0	TSA	11	0.13	0.76	51.7	0.75	0.62	0.66
C_Asia	DMI	6	−0.60	89.9	TASI	7	−0.63	0.80	73.1	0.81	0.45	0.55
NE_Asia	NINO12	5	0.89	44.5	SETIO	7	−0.58	0.92	44.7	0.95	0.52	0.73
SE_Asia	NINO12	4	0.81	53.6	TSA	6	0.30	0.90	50.0	0.88	0.86	0.77
SH_EQAS	NINO34	3	0.82	65.4	WTIO	11	−0.68	0.86	63.7	0.94	0.54	0.83
Australia	NINO4	10	−0.69	159.3	SWIO	6	0.37	0.80	149.9	0.79	0.70	0.68

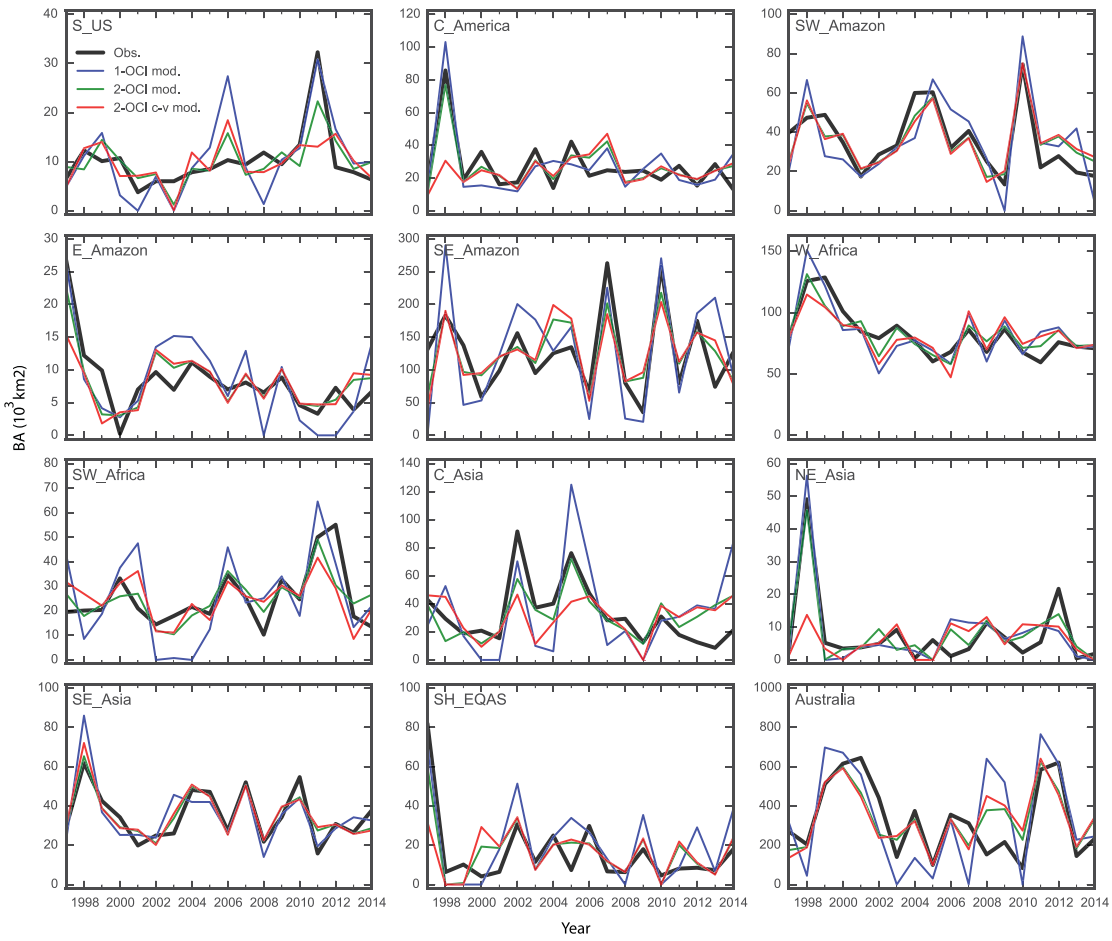

Figure 4. Comparison of observed and predicted annual burned area in 12 globally distributed hotspot regions. The predicted results from three models, the 1-OCI model, the 2-OCI model, the 2-OCI cross validation (c-v) model, are shown.

outlooks for a broader continental-scale region encompassing most of the southern hemisphere equatorial Asia. Similarly, in South America our analysis suggests that it may be possible to develop fire forecasts for savannas and seasonally dry forests in southeastern Brazil, outside of the current domain of the UC Irvine fire outlook system developed for the Amazon (http://www.ess.uci.edu/~amazonfirerisk/ForecastWeb/SAMFSS.html).

Other hotspots we uncovered may present new opportunities to manage ecosystem processes and air quality. For example, the hotspot in northeastern Asia (NE_Asia) overlaps with Siberian forests that provide habitat for the endangered Amur tiger (Carroll and Miquelle 2006). A long lead time for the regression model this region (table 2) may enable land managers to more effectively manage fire risk in important conservation areas. In the southern US (SE_US), prescribed and wildland fires contribute to elevated ozone and particulate matter levels during spring, summer, and fall (Zhang *et al* 2014). Understanding the fire danger exerted by climate before the onset of the fire season may help state air quality agencies optimize mitigation strategies and adjust emissions from other sectors to meet the newly lowered US National Ambient Air Quality Standards for ground-level ozone. In Central America, expansion and intensification of agriculture has increased anthropogenic pressure on protected areas and national parks (e.g. Fagan *et al* 2013). The development of an early warning fire system in this region may allow managers to allocate fire suppression resources more efficiently and to create incentive programs to limit anthropogenic fire use during periods of extreme risk.

The hotspot regions in this study capture important coherence in fire–climate relationships, but the spatial scale of our analysis may be too coarse for some applications. Some areas where the climate–fire relationships have been extensively explored, such as in the western US and tropical Africa, were not classified as hotspot regions in this study because they are small or exhibit a heterogeneous response to OCI variability. With respect to the development of operational forecasts in hotspot regions, another important step is to tailor the regions of SST influence to optimize model performance (figure S7).

4.2. ENSO as a global driver of burned area dynamics

ENSO is the primary large-scale climate mode that influences global fire activity and provides the foundation for predictability in the global fire system. Previous studies have highlighted some aspects of the ENSO influence on global fires (e.g. van der Werf *et al* 2004, Marlier *et al* 2013), but this study is the first comprehensive assessment of OCI–fire relationships over multiple ENSO cycles. ENSO is phase locked with the seasonal cycle (McPhaden *et al* 2006), intensifies in predictable ways from northern hemisphere summer through fall and early winter, and forces ocean-atmosphere dynamics (with time delays) in other regions (figure S3). Subsequent changes in regional climate in fire prone regions, and the influence of this climate variability on fuel characteristics serves as the physical basis for the statistical relationships we identified here.

Fire is a critical component of the Earth system response to ENSO-driven changes in tropical temperature and precipitation (Keppel-Aleks *et al* 2014). Although ENSO is the dominant mode of climate variability for the growth rate of atmospheric CO_2 and global burned area, this study highlights the broad influence of OCIs from all three ocean basins as a driver of terrestrial ecosystem processes. Atlantic and Indian OCI variability also contributed directly to burned area dynamics in North and South America and western Africa, and most regions exhibited a dual sensitivity to OCI variability from different ocean basins. Both of these findings suggest improved representation and evaluation of OCI–fire linkages is needed in Earth system models used to assess climate-carbon cycle feedbacks.

4.3. Uncertainties and future directions

Fire–climate interactions vary considerably across biomes and continents, complicating efforts to derive consistent predictive relationships. In some areas, fire activity may be negatively influenced by precipitation during the fire season, yet positively affected by precipitation during the preceding wet season (Archibald *et al* 2009). The simultaneous influence of precipitation on fuel moisture and fuel amount may reduce fire predictability using the approach described here, which relied upon OCI information with a single fixed lead time. Development of more sophisticated modeling approaches, such as regression models representing both positive and negative correlations between burned area and OCIs, models that integrate information from OCIs in the same basin across a period of several months, or nonlinear models that capture the non-monotonic fire responses to climate, are important next steps that will require the use of longer and higher resolution burned area time series for model development and validation. Longer burned area time series spanning strong El Niño years (including the ongoing 2015–2016 El Niño) may also help simulate fire extremes more accurately by avoiding the dominance of a single event in the time series (see section 3.3). We note that anthropogenic forcing of the climate system may create new climate modes or modify the strength of many existing teleconnections that are important for the fire prediction models described here. This changing baseline necessitates the development of an adaptive forecasting approach that allows for periodic refinements to model structure and parameters, and the exploration of approaches that predict fire and ecosystem variables using meteorological variables from coupled dynamical forecasting systems.

It is also critical to recognize that climate is not the sole factor determining the spatiotemporal variability of the burned area (Archibald *et al* 2013, Lehmann *et al* 2014). Fire regimes, as defined by the processes regulating ignition, intensity, spread rate, size, and severity, are influenced by many forms of human activity (Archibald *et al* 2010, Le Page *et al* 2010). Land management may considerably amplify the climate sensitivity of fire activity (e.g. Field *et al* 2009, Morton *et al* 2013), or contribute to trends and variability that are not closely coupled with the climate system (Andela and van der Werf 2014). In the latter case, changes in land use that are not closely coupled with the climate system could significantly contribute to trends and variability. To better represent the influence of humans on global fire dynamics, greater investment is needed with respect to the development of long-term, internally consistent annual time series of human system variables, including population density, cropland areas and yields, and road networks.

5. Conclusions

Previous studies have demonstrated that robust seasonal predictions of fire activity can be made in specific regions. For the first time, we explored the degree to which SSTs in different ocean basins can explain year to year variations in burned area at a global scale, with lead times enabling the development of operational fire forecasts. We found about half of global burned area can be predicted with a lead time of 3 or more months. Central America and equatorial Asia had the highest levels of predictability, in part from the strong sensitivity of fires in these regions to forcing from ENSO. Use of two OCIs from different ocean basins considerably improved model performance in many regions. Twelve hotspot regions were identified globally where fires may be predicted with moderate confidence levels. Several of these hotspots were in areas that have not been targeted in past work for forecast development, suggesting that new opportunities may exist for improving fire and ecosystem management. Collectively, the strong influence of OCI variability on global burned area highlights the

diversity of climate–fire teleconnections on seasonal timescales and the opportunity to investigate mechanisms that couple climate and fire in the Earth system.

Acknowledgments

This work would not have been possible without near real-time access to ocean climate indices provided by NOAA's State of the Ocean climate program (http://stateoftheocean.osmc.noaa.gov) and past NASA investment in the Earth Observing System and the Global Fire Emissions Database. This research was supported by a grant to Randerson from the Gordon and Betty Moore Foundation (GBMF3269) and to Morton from NASA's Interdisciplinary Research in Earth Science Program.

References

Akaike H 1974 New look at statistical-model identification *IEEE Trans. Autom. Control* **19** 716–23

Alencar A, Asner G P, Knapp D and Zarin D 2011 Temporal variability of forest fires in eastern Amazonia *Ecological Appl.* **21** 2397–412

Alley W M 1984 The Palmer drought severity index: limitations and assumptions *J. Clim. Appl. Meteorol.* **23** 1100–9

Andela N and van der Werf G R 2014 Recent trends in African fires driven by cropland expansion and El Nino to La Nina transition *Nat. Clim. Change* **4** 791–5

Aouizerats B, van der Werf G R, Balasubramanian R and Betha R 2015 Importance of transboundary transport of biomass burning emissions to regional air quality in Southeast Asia during a high fire event *Atmos. Chem. Phys.* **15** 363–73

Archibald S, Lehmann C E R, Gómez-Dans J L and Bradstock R A 2013 Defining pyromes and global syndromes of fire regimes *Proc. Natl Acad. Sci.* **110** 6442–7

Archibald S, Nickless A, Govender N, Scholes R J and Lehsten V 2010 Climate and the inter-annual variability of fire in southern Africa: a meta-analysis using long-term field data and satellite-derived burnt area data *Glob. Ecology Biogeography* **19** 794–809

Archibald S, Roy D P, van Wilgen B W and Scholes R J 2009 What limits fire? An examination of drivers of burnt area in Southern Africa *Glob. Change Biol.* **15** 613–30

Barbero R, Moron V, Mangeas M, Despinoy M and Hely C 2011 Relationships between MODIS and ATSR fires and atmospheric variability in New Caledonia (SW Pacific) *J. Geophys. Res.-Atmos.* **116** D21110

Carroll C and Miquelle D G 2006 Spatial viability analysis of Amur tiger Panthera tigris altaica in the Russian Far East: the role of protected areas and landscape matrix in population persistence *J. Appl. Ecology* **43** 1056–68

Chen Y, Randerson J T, Morton D C, DeFries R S, Collatz G J, Kasibhatla P S, Giglio L, Jin Y and Marlier M E 2011 Forecasting fire season severity in South America using sea surface temperature anomalies *Science* **334** 787–91

Chen Y, Velicogna I, Famiglietti J S and Randerson J T 2013 Satellite observations of terrestrial water storage provide early warning information about drought and fire season severity in the Amazon *J. Geophys. Res.: Biogeosci.* **118** 495–504

Dixon P G, Goodrich G B and Cooke W H 2008 Using teleconnections to predict wildfires in Mississippi *Mon. Weather Rev.* **136** 2804–11

Duffy P A, Walsh J E, Graham J M, Mann D H and Rupp T S 2005 Impacts of large-scale atmospheric–ocean variability on Alaskan fire season severity *Ecological Appl.* **15** 1317–30

Fagan M E, DeFries R S, Sesnie S E, Arroyo J P, Walker W, Soto C, Chazdon R L and Sanchun A 2013 Land cover dynamics following a deforestation ban in northern Costa Rica *Environ. Res. Lett.* **8** 034017

Fernandes K *et al* 2011 North Tropical Atlantic influence on western Amazon fire season variability *Geophys. Res. Lett.* **38** L12701

Field R D and Shen S S P 2008 Predictability of carbon emissions from biomass burning in Indonesia from 1997 to 2006 *J. Geophys. Res.-Biogeosci.* **113** G04024

Field R D, van der Werf G R and Shen S S P 2009 Human amplification of drought-induced biomass burning in Indonesia since 1960 *Nat. Geosci.* **2** 185–8

Field R D *et al* 2015 Development of a global fire weather database *Nat. Hazard Earth Syst.* **15** 1407–23

Fuller D O and Murphy K 2006 The ENSO-fire dynamic in insular Southeast Asia *Clim. Change* **74** 435–55

Giglio L, Randerson J T and Van der Werf G R 2013 Analysis of daily, monthly, and annual burned area using the fourth-generation global fire emissions database (GFED4) *J. Geophysi. Res.: Biogeosci.* **118** 317–28

Giglio L, van der Werf G R, Randerson J T, Collatz G J and Kasibhatla P 2006 Global estimation of burned area using MODIS active fire observations *Atmos. Chem. Phys.* **6** 957–74

Goodrick S L and Hanley D E 2009 Florida wildfire activity and atmospheric teleconnections *Int. J. Wildland Fire* **18** 476–82

Gudmundsson L, Rego F C, Rocha M and Seneviratne S I 2014 Predicting above normal wildfire activity in southern Europe as a function of meteorological drought *Environ. Res. Lett.* **9** 084008

Hessl A E 2011 Pathways for climate change effects on fire: Models, data, and uncertainties *Prog. Phys. Geog.* **35** 393–407

Kao H Y and Yu J Y 2009 Contrasting eastern-Pacific and central-Pacific types of ENSO *J. Clim.* **22** 615–32

Keppel-Aleks G, Wolf A S, Mu M, Doney S C, Morton D C, Kasibhatla P S, Miller J B, Dlugokencky E J and Randerson J T 2014 Separating the influence of temperature, drought, and fire on interannual variability in atmospheric CO_2 *Glob. Biogeochemical Cycles* **28** 1295–310

Kitzberger T, Brown P M, Heyerdahl E K, Swetnam T W and Veblen T T 2007 Contingent Pacific—Ocean influence on multicentury wildfire synchrony over western North America *Proc. Natl Acad. Sci. USA* **104** 543–8

Le Page Y, Oom D, Silva J M N, Jonsson P and Pereira J M C 2010 Seasonality of vegetation fires as modified by human action: observing the deviation from eco-climatic fire regimes *Glob. Ecology Biogeography* **19** 575–88

Lehmann C E R *et al* 2014 Savanna vegetation–fire–climate relationships differ among continents *Science* **343** 548–52

Liu Y Q 2006 North Pacific warming and intense northwestern US wildfires *Geophys. Res. Lett.* **33** L21710

Macias Fauria M and Johnson E A 2006 Large-scale climatic patterns control large lightning fire occurrence in Canada and Alaska forest regions *J. Geophys. Res.: Biogeosci.* **111** G04008

Macias Fauria M and Johnson E A 2008 Climate and wildfires in the North American boreal forest *Phil.Trans. R. Soc.* B **363** 2317–29

Marcos R, Turco M, Bedía J, Llasat M C and Provenzale A 2015 Seasonal predictability of summer fires in a Mediterranean environment *Int. J. Wildland Fire* **24** 1076–84

Marlier M E, DeFries R S, Voulgarakis A, Kinney P L, Randerson J T, Shindell D T, Chen Y and Faluvegi G 2013 El Nino and health risks from landscape fire emissions in southeast Asia *Nat. Clim. Change* **3** 131–6

McPhaden M J, Zebiak S E and Glantz M H 2006 ENSO as an integrating concept in Earth science *Science* **314** 1740–5

Morton D C, Le Page Y, DeFries R, Collatz G J and Hurtt G C 2013 Understorey fire frequency and the fate of burned forests in southern Amazonia *Phil. Trans. R. Soc.* B **368** 20120163

Pena J M, Lozano J A and Larranaga P 1999 An empirical comparison of four initialization methods for the K-means algorithm *Pattern Recogn. Lett.* **20** 1027–40

Preisler H K and Westerling A L 2007 Statistical model for forecasting monthly large wildfire events in western United States *J. Appl. Meteorol. Clim.* **46** 1020–30

Preisler H K, Westerling A L, Gebert K M, Munoz-Arriola F and Holmes T P 2011 Spatially explicit forecasts of large wildland

fire probability and suppression costs for California *Int. J. Wildland Fire* **20** 508–17
Randerson J T, Chen Y, van der Werf G R, Rogers B M and Morton D C 2012 Global burned area and biomass burning emissions from small fires *J. Geophys. Res.-Biogeosci.* **117** G04012
Reid J S, Xian P, Hyer E J, Flatau M K, Ramirez E M, Turk F J, Sampson C R, Zhang C, Fukada E M and Maloney E D 2012 Multi-scale meteorological conceptual analysis of observed active fire hotspot activity and smoke optical depth in the Maritime Continent *Atmos. Chem. Phys.* **12** 2117–47
Riano D, Ruiz J A M, Martinez J B and Ustin S L 2007 Burned area forecasting using past burned area records and Southern Oscillation Index for tropical Africa (1981–1999) *Remote Sens. Environ.* **107** 571–81
Roads J, Fujioka F, Chen S and Burgan R 2005 Seasonal fire danger forecasts for the USA *Int. J. Wildland Fire* **14** 1–18
Roads J, Tripp P, Juang H, Wang J, Fujioka F and Chen S 2010 NCEP-ECPC monthly to seasonal US fire danger forecasts *Int. J. Wildland Fire* **19** 399–414
Schoennagel T, Veblen T T, Romme W H, Sibold J S and Cook E R 2005 Enso and pdo variability affect drought-induced fire occurrence in Rocky Mountain subalpine forests *Ecological Appl.* **15** 2000–14
Shabbar A, Skinner W and Flannigan M D 2011 Prediction of seasonal forest fire severity in Canada from large-scale climate patterns *J. Appl. Meteorol. Clim.* **50** 785–99
Skinner W R, Shabbar A, Flannigan M D and Logan K 2006 Large forest fires in Canada and the relationship to global sea surface temperatures *J. Geophys. Res.-Atmos.* **111** D14106
Spessa A C, Field R D, Pappenberger F, Langner A, Englhart S, Weber U, Stockdale T, Siegert F, Kaiser J W and Moore J 2015 Seasonal forecasting of fire over Kalimantan, Indonesia *Nat. Hazards Earth Syst. Sci.* **15** 429–42
van der Kaars S, Tapper N and Cook E J 2010 Observed relationships between El Nino-Southern Oscillation, rainfall variability and vegetation and fire history on Halmahera, Maluku, Indonesia *Glob. Change Biol.* **16** 1705–14
van der Werf G R, Randerson J T, Collatz G J, Giglio L, Kasibhatla P S, Arellano A F, Olsen S C and Kasischke E S 2004 Continental-scale partitioning of fire emissions during the 1997 to 2001 El Nino/La Nina period *Science* **303** 73–6
van der Werf G R, Randerson J T, Giglio L, Collatz G J, Kasibhatla P S and Arellano A F 2006 Interannual variability in global biomass burning emissions from 1997 to 2004 *Atmos. Chem. Phys.* **6** 3423–41
van der Werf G R, Randerson J T, Giglio L, Collatz G J, Mu M, Kasibhatla P S, Morton D C, DeFries R S, Jin Y and van Leeuwen T T 2010 Global fire emissions and the contribution of deforestation, savanna, forest, agricultural, and peat fires (1997–2009) *Atmos. Chem. Phys.* **10** 11707–35
van der Werf G R *et al* 2008 Climate regulation of fire emissions and deforestation in equatorial Asia *Proc. Natl Acad. Sci. USA* **105** 20350–5
von Storch H and Zwiers F W 2001 *Statistical Analysis in Climate Research* (Cambridge: Cambridge University Press)
Westerling A L, Gershunov A, Cayan D R and Barnett T P 2002 Long lead statistical forecasts of area burned in western US wildfires by ecosystem province *Int. J. Wildland Fire* **11** 257–66
Westerling A L, Hidalgo H G, Cayan D R and Swetnam T W 2006 Warming and earlier spring increase western US forest wildfire activity *Science* **313** 940–3
Wooster M J, Perry G L W and Zoumas A 2012 Fire, drought and El Nino relationships on Borneo (Southeast Asia) in the pre-MODIS era (1980–2000) *Biogeosciences* **9** 317–40
Zhang Y, Wang W, Wu S Y, Wang K, Minoura H and Wang Z F 2014 Impacts of updated emission inventories on source apportionment of fine particle and ozone over the southeastern US *Atmos. Environ.* **88** 133–54